Structure and Properties of Hexa- and Undecablock Terpolymers with Hierarchical Molecular Architectures

Guillaume Fleury and Frank S. Bates*

Department of Chemical Engineering and Materials Science, University of Minnesota, Minneapolis, Minnesota 55455

Received January 28, 2009; Revised Manuscript Received March 14, 2009

ABSTRACT: We report the synthesis, phase behavior, and viscoelastic and mechanical properties of a new type of multiblock copolymer composed of glassy poly(cyclohexylethylene) (C), semicrystalline poly(ethylene) (E), and elastomeric poly(ethylene-*alt*-propylene) (P). Five nearly monodisperse CECEC−P hexablock terpolymers and one $(CECEC)_2$−P undecablock copolymer were synthesized by sequential anionic polymerization followed by catalytic hydrogenation. These multiblock copolymers, which contain equal volume fractions of P and compositionally symmetric CECEC, microphase separate by two different processes: segregation induced by crystallization of the E blocks and through chemical incompatibility between C, E, and P. These materials contain two different complex morphologies each with two length scales determined by the local (C−E) and overall (C−E−P) order−disorder transition temperatures relative to the glass and crystallization temperatures of the C and E blocks, respectively. Structure was determined by SAXS, TEM, and mechanical spectroscopy. Tensile tests reveal that the hexablock copolymers are tough (ca. ≥750% strain at break) and exhibit high elastic recovery despite the presence of P domains comprised of loose elastomeric end blocks. The $(CECEC)_2$−P undecablock, which orders from the homogeneous melt as a consequence of crystallization of the E blocks, exhibits roughly three times the stress at failure without the loss of other physical properties. These results offer new insights into the development of enhanced mechanical response based on hierarchical molecular design.

Introduction

Self-assembly of multiblock copolymers has been exploited by many researchers and industrialists to generate materials with enhanced composite mechanical properties.[1−3] The mechanical response of these products can be tuned by varying the molecular architecture (i.e., the molecular weight, the volume fractions of each constituent, and the chain topology) and the sequence of blocks. For example, for over 3 decades commercial products in footwear, pressure-sensitive adhesives, and asphalt modifiers[1] have benefitted from poly(styrene)-based block copolymers[2,3] such as poly(styrene-*b*-butadiene-*b*-styrene) (SBS) and poly(styrene-*b*-isoprene-*b*-styrene) (SIS). These compounds exhibit a composite mechanical response reflecting both the glassy (S) and rubbery (B or I) properties due to a microphase-separated structure. In these applications, the hard domains serve as thermally reversible cross-links that produce efficient elastic strain and recovery at room temperature. Numerous studies have established the origins of the improvement in mechanical properties[4−10] of such thermoplastic elastomers relative to the homologous homopolymer blends. At small strains, the response of the material is mainly governed by the microdomain structure and slippage of trapped entanglements in the rubbery middle block,[1,7] while at large strains, microdomain structural disruption (grain rotation, buckling and chevron formation) leads to a mechanical response controlled by chain elongation and orientation.[4,9,10] However, this class of block copolymers has several deficiencies including oxidative, thermal and chemical instabilities due to unsaturation in the soft blocks[11] and a low upper service temperature (UST) established by the glass transition temperature of the poly(styrene) blocks (ca. 100 °C).

Some of these shortcomings can be mitigated or eliminated by catalytic hydrogenation without compromising essential properties.[12] However, although poly(cyclohexylethylene) (C), obtained by the hydrogenation of poly(styrene), exhibits a higher glass transition temperature[13] (ca. 147 °C) this desirable feature is accompanied by a large entanglement molecular weight[14] (M_e = 40 kg·mol^{-1}), which makes the glassy polymer very brittle. Poly(cyclohexylethylene) can be combined with other saturated hydrocarbon polymers to produce hybrid saturated block copolymers with rubbery (e.g., poly(ethylene-*alt*-propylene) (P) or poly(ethylethylene) (E_E)) or semicrystalline (poly(ethylene) (E)) blocks, through the hydrogenation of poly(isoprene), poly(1,2-butadiene), or poly(1,4-butadiene), respectively. This commercially viable technology offers an attractive way to create new function while avoiding the aforementioned complications. In this way enhanced toughness relative to the fracture behavior of C homopolymers can be achieved along with robust control over mechanical behavior (from elastomeric to plastic) through manipulation of the composition and block architecture (sequencing), molecular weight, and distribution of glassy, rubbery and semicrystalline domains. These polyolefin block copolymers are attractive for many applications requiring a high UST and good stability toward oxidative, thermal or UV degradation.[10]

Simple (e.g., AB or ABA) block copolymers usually show a single periodic morphology that depends on the molecular characteristics and architecture. Linear AB diblocks[15−19] and ABA triblocks[20−30] have been studied most extensively along with $(AB)_n$ star[31] and multiblock[32−35] types. During the past two decades ABC triblock terpolymers have gained popularity in the research community leading to an explosion in the catalogue of documented ordered phase morphologies. Block copolymer blends containing all combinations of these individual types can generate additional self-assembled structures, which may contain multiple periodicities such as a noncentrosymmetric superlattice[36] or complex morphologies like the "knitting" pattern.[37,38]

Hierarchical structures from block copolymer systems offer promising avenues for tuning optical, mechanical, transport, and many other material properties. Applications requiring structures with different length scales, such as photonic crystals,[39] can be conceived from a material built with two different periodicities.

* To whom correspondence should be addressed: E-mail: bates@cems.umn.

10.1021/ma900183p CCC: $40.75
Published on Web 04/20/2009

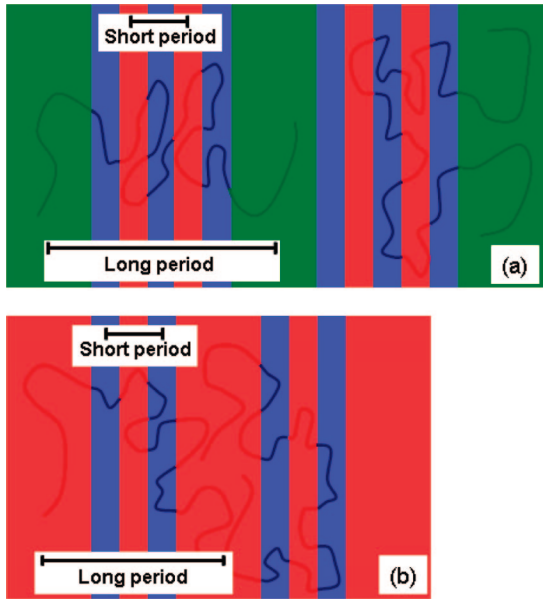

Figure 1. Schematic representation of the doubly periodic lamellar mesostructure adopted by (a) V′ISISISISIV′ and (b) S′ISISISISIS′ undecablock copolymers as reported by Matsushita et al.[45,46] Domains correspond to V (green) = poly(2-vinylpyridine), I (blue) = poly(isoprene), and S (red) = poly(styrene).

One of the earliest reports of a hierarchical structure from a block copolymer system was presented by ten Brinke et al.[40−42] who synthesized a supramolecular graft copolymer from a poly(styrene-*b*-4-vinylpyridine) with short hydrogen-bonded side blocks of pentadecylphenol linked to the poly(4-vinylpyridine) chains. Self-organized structures-in-structures were obtained with two different length scales, i.e., one corresponding to the segregation between the poly(styrene) and the poly(4-vinylpyridine) blocks and the other related to the poly(4-vinylpyridine)/pentadecylphenol hydrogen-bonded complex. Following the same supramolecular approach Chiang et al. has recently synthesized comb−coil block copolymers exhibiting two distinct mesophases.[43,44] Matsushita et al. has prepared materials containing two distinct lamellar structures,[45−47] based on a new concept: highly asymmetric S′ISISISISIS′[45] ($M_{n,S'} \approx 5M_{n,S} \approx 5M_{n,I}$) and VISISISISIV[46] ($M_{n,V} \approx 5M_{n,I} \approx 5M_{n,S}$) undecablock copolymers (Here V denotes poly(2-vinylpyridine); we have substituted V for P as used by Matsushita et al. to avoid confusion with our nomenclature). In the case of V′ISISISISIV′, the hierarchical doubly periodic lamellar structure consists of thick V domains sequenced with five layer regions comprised of three I and two S lamellae, while S′ISISISISIS′ microphase segregates into a doubly periodic parallel lamellar structure with alternating thick S domains and three layer sections of two I and one S lamellae as shown in Figure 1. Theoretical studies[48−54] based on both weak segregation theory[52] and self-consistent mean field theory[53,54] have accounted for these lamellae-in-lamellae morphologies.

We believe the opportunities created by architecturally complex block copolymers are largely untapped. Moreover, such compounds need not be relegated solely to the research community. Many monomers can be configured into a plethora of architectural designs using conventional anionic and other controlled polymerization techniques, and in many instances these methods can be readily scaled to commercial practice. We have been exploring relatively simple combinations of C, P, E, and E_E blocks in linear multiblock copolymer configurations for several years. Of particular interest is the manipulation of mechanical properties in these materials, including the tensile elastic modulus, yield stress, stress and strain at break, and elastic recovery. One molecular design, CECEC, has been particularly successful at imparting outstanding fracture toughness to the otherwise brittle, glassy, poly(cyclohexylethylene).

Scheme 1. Molecular Structure of SBSBS−I Hexablock Copolymers

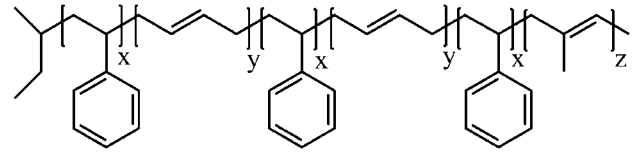

In this article we describe initial findings obtained from a new class of saturated multiblock copolymers, CECEC−P and $(CECEC)_2$−P containing 50% P, 25% C, and 25% E. Our molecular design was inspired in part by the beautiful results reported by Matsushita and co-workers.[45−47] Although not discussed in this report, our choice of architecture anticipates a future development of nanoporous yet mechanically tough membranes based on the $(ABABA)_n$−C design. Prior success with CECEC copolymers motivated us to investigate whether mechanic integrity, particularly toughness, is preserved when an equal volume fraction of singly tethered and liquid-like P is dispersed between intrinsically tough layers of the pentablock copolymer. Two limiting cases are examined: (*i*) C and E microphase separation is induced from a thermodynamically homogeneous state by E block crystallization; (*ii*) microphase separation induced by chemical incompatibility precedes crystallization. We have characterized the resulting structures by small-angle X-ray scattering (SAXS) and transmission electron microscopy and mechanical behavior by tensile testing. Finally, a single $(CECEC)_2$−P undecablock copolymer, obtained by coupling hexablocks, was investigated to assess the role of singly versus doubly tethered P blocks in the first category.

Experimental Section

Block Copolymer Synthesis, Molecular Characterization, and Hydrogenation. The multiblock copolymers used in this study were synthesized by sequential anionic polymerization of styrene (S), butadiene (B), and isoprene (I) using techniques described elsewhere[55] to produce precursor SBSBS−I block copolymers (Scheme 1). The polymerization was initiated with sec-butyllithium in purified cyclohexane at 40 °C and an aliquot of the first block was isolated after 8 h and saved for further analysis before proceeding with the subsequent sequence of monomer additions. An SBSBS−I−SBSBS undecabock copolymer was obtained by coupling living SBSBS−I^-,Li^+ hexablock chains using α,α′-dibromo-p-xylene. The number average molecular weight (M_n) and molecular weight distribution (M_w/M_n) of the initial poly(styrene) blocks and the completed block copolymers were determined by size-exclusion chromatography (SEC) using a Waters 717 GPC equipped with three Polymer Laboratories Mixed-C columns calibrated with narrow molecular weight distribution polystyrenes as standards operated at 25 °C with tetrahydrofuran (THF) at a flow rate of 1 $mL \cdot s^{-1}$.

Quantitative ^1H NMR spectra of the unsaturated block copolymers dissolved in $CDCl_3$ were recorded on a Varian Unity Inova 300 spectrometer with a pulse repetition delay of 20 s to determine the volume fractions of poly(styrene), poly(butadiene) and poly(isoprene). ^1H NMR spectra (see Supporting Information for the ^1H NMR spectra of SBSBS−I_120k (Figure S1)) established that the butadiene polymerizations resulted in a high degree of 1,4-regioselectivity with 6−8 mol % of 1,2-insertions while the isoprene polymerizations produced a predominantly 4,1-insertion with 5−7 mol % of 4,3-insertions. Block mole fractions were obtained using the integrated ^1H NMR spectra and converted to volume fractions f_S, f_B and f_I using published homopolymer densities at 140 °C ($\rho_I = 0.830$, $\rho_S = 0.969$, $\rho_B = 0.826$ g/cm^3),[14] allowing us to calculate the block volume fractions for the unsaturated block copolymers.

Scheme 2. Molecular Structure of CECEC−P Hexablock Copolymers

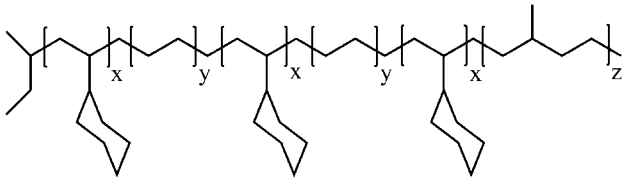

Monodisperse CECEC−P block copolymers (Scheme 2) were obtained by catalytic hydrogenation of SBSBS−I over a silica-supported Pt/Re catalyst[12] (supplied by Dow Chemicals Co.) in degassed cyclohexane at 170 °C under 500 psig of H_2 for 12 h. The extent of hydrogenation, always >98% for the polymers discussed here, was determined by ^{1}H NMR spectroscopy in deuterated toluene C_7D_8 at 70 °C using a Varian Inova 300 spectrometer (see Supporting Information for the ^{1}H NMR spectra of CECEC−P_120k (Figure S2)). SEC chromatograms recorded on a PL-GPC 220 system at 140 °C in 1,2,4-trichlorobenzene show narrow molecular chain distributions, devoid of evidence of chain degradation. The molecular weight M_n and the volume fractions f_C, f_E, and f_P were calculated from the composition data for the unsaturated polymers and the molecular weight of the initial S block, along with bulk homopolymer densities[14] at 140 °C ($\rho_P = 0.79$, $\rho_C = 0.92$, $\rho_E = 0.78$ g/cm^3) and assuming complete hydrogenation. The molecular parameters for each block copolymer used in this study are listed in Table 1.

Dynamical Mechanical Spectroscopy. Viscoelastic spectra were obtained from the saturated multiblock copolymers by dynamical mechanical spectroscopy using a Rheometrics Scientific ARES strain-controlled rheometer fitted with 25 mm diameter parallel plates. All measurements were conducted under a nitrogen atmosphere in the linear vicoelastic regime, as determined from dynamic strain sweep tests performed at 140 °C. The dynamic elastic (G') and loss (G'') moduli were measured as a function of temperature at a frequency $\omega = 0.05$ rad·s^{-1} and a strain $\gamma = 1$ to 2.5%; these experiments, referred to as isochronal temperature ramp tests, were employed to search for order−disorder or other phase transitions between the poly(cyclohexylethylene) $T_{g,C}$ ($\approx$ 140 °C) and 300 °C. Isothermal frequency data was obtained at frequencies of $100 \leq \omega \leq 0.01$ rad·s^{-1} also with $\gamma = 1$ to 2.5% and at select temperatures.

Large Amplitude Reciprocating Shear Alignment. The reciprocating shear device described by Koppi et al.[18] was employed to orient 20 mm × 20 mm × 1 mm compression-molded samples at 250 °C using a strain amplitude of 200% and a shear rate of 0.5 s^{-1}; samples were processed under argon for 12 h. After shearing, the sample was cooled to room temperature over a 2 h period. This procedure improves the degree of long-range order, which often facilitates characterization of multiblock copolymers by SAXS or TEM.

Thermal Analysis. Differential scanning calorimetry (DSC) was performed using a TA Instruments Q1000 DSC. The thermal history of each sample was erased by heating to 170 °C for 10 min before cooling to −80 at 10 °C/min. The reported percent crystallinity and the peak melting temperature of the E blocks were collected during the second heating run from −80 to +150 °C at a temperature ramp rate of 10 °C/min. The crystallinity, X_c, was calculated from the heat of melting ΔH_m using the expression $X_c = (\Delta H_m/w_E)\rho H^0_{m,E}$ where w_E is the E weight fraction and $\Delta H^0_{m,E} = 277$ J·g^{-1} is the theoretical heat of melting for perfectly crystalline poly(ethylene).[55]

Transmission Electron Microscopy (TEM). TEM images of the multiblock copolymers were acquired using a JEOL 1210 transmission electron microscope operating at 120 kV in the bright field mode. Samples were prepared and stained according to established procedures.[57] Samples were cryo-microtomed at −120 °C using a diamond knife to create a flat surface then stained by exposure to ruthenium tetroxide (RuO_4) vapors to create contrast between different microdomains. Stained thin sections (60−90 nm) were then produced by again microtoming at −120 °C for subsequent TEM analysis.

Small Angle X-ray Scattering (SAXS). Synchrotron SAXS experiments were conducted at Argonne National Laboratory using the equipment maintained by the DuPont−Northwestern−Dow Collaborative Access Team (DND−CAT). Two equipment setups were employed: (1) an X-ray wavelength (λ) of 1.032 Å with a sample-to-detector distance of 2.01 m and (2) $\lambda = 0.886$ Å with a sample-to-detector distance of 5.47 m. Both distances were calibrated with silver behenate and data were acquired on a Mar CCD area detector. Sample temperature was controlled using a liquid-N_2 cooled DSC chamber under a helium purge. All samples were heated to 250 °C for 5 min before data was acquired in an effort to erase effects due to thermal history. Samples were cooled and held at target temperatures for 5 min prior to data collection. Two dimensional scattering patterns were azimuthally averaged and are presented in this Article as intensity I versus scattering wavevector modulus q ($q = |\mathbf{q}| = (4\pi/\lambda)\sin(\theta/2)$, where θ is the scattering angle).

Tensile Testing. Uniaxial tensile stress was obtained as a function of applied strain using a Rheometrics Scientific MINIMAT equipped with a 200 N load cell and operating at 22 °C with a length-independent strain rate of 0.0015 s^{-1} (i.e., constant crosshead velocity to achieve a single strain rate) for all the block copolymers. Rectangular tensile bars measuring 20 mm × 3 mm × 2 mm were used with an initial gage length of 5 mm. Force-displacement measurements were converted to engineering stress $\sigma = F/A_0$ versus the nominal strain $\varepsilon = (l - l_0)/l_0$), where A_0 and l_0 are respectively the initial cross-sectional area and the length of the samples. The Young's modulus E was determined by fitting the linear elastic portion of the stress−strain curve below the yield point. All reported data reflect an average over a minimum of six trials. Cyclic tensile−compression tests were conducted at 22 °C using the MINIMAT at a strain rate of 0.0015 s^{-1}. These experiments employed the following protocol. First, a specimen was stretched up to a strain of 600% (500% for CECEC−P_77k and CECEC−P_85k due to smaller strains at break). Then the applied force was unloaded and the sample was compressed back to its initial 5 mm gage length. This loading and unloading sequence was repeated for a total of six cycles. Finally, the specimen was strained to failure. Samples were not removed from the testing apparatus between cycles.

Results and Analysis

Synthesis. A series of high molecular weight SBSBS−I copolymers was synthesized by sequential anionic polymerization and hydrogenated to produce "symmetric" CECEC−P hexablock copolymers. Block copolymer compositions were established by ^{1}H NMR obtained from the SBSBS−I precursors.[58] The SBSBS−I SEC traces each contain evidence of a small amount of SBSBS (≤5%) and a very low proportion of coupled SBSBSISBSBS (≤1%). The extent of coupling for the SBSBS−I−SBSBS undecablock copolymer was determined using SEC and was determined to be 90%. Complete hydrogenation (>98%) of the parent SBSBS−I or SBSBS−I−SBSBS is marked by the disappearance of specific resonances associated with the aromatic protons (6.2−7.2 ppm) and the vinyl protons (4.8−5.4 ppm) in the ^{1}H NMR spectra of the saturated CECEC−P and $(CECEC)_2$−P. Saturation by hydrogenation of these polymers did not significantly influence the polydispersity of the samples. The CECEC−P hexablocks were designed to have equal volumes of CECEC and P, and equal volumes of C and E (i.e., $f_C \sim f_E \sim {}^1/_2 f_P$) over molecular weights between 76.6 and 150.5 kg·mol^{-1}. The molecular characteristics for the CECEC−P compounds are provided in Table 1.

Isothermal frequency sweep tests were performed at individual temperatures between 140 and 300 °C, and the G' and G'' data were shifted along the frequency axis to form pseudomaster curves as illustrated in Figure 2, where the reference temperature is 160 °C. Kossuth et al.[60] demonstrated

Table 1. Molecular Characterization Data for CECEC−P and $(CECEC)_2$−P Copolymers

sample	M_n(kg/mol)	M_w/M_n[a]	f_C	f_E	f_P	N_0[b]	T_{ODT}[c] (°C)	X_c[d] (%)	$T_{m,E}$[f] (±1 °C)	T_g[c] (±1 °C)
CECEC−P_77k	76.6	1.10	0.25	0.25	0.5	1312	<140	15	93	123
CECEC−P_85k	84.6	1.09	0.26	0.24	0.5	1447	<140	16	94	123
CECEC−P_100k	100.8	1.07	0.31	0.2	0.49	1711	>300	13	88	127
CECEC−P_120k	119.6	1.09	0.25	0.25	0.5	2048	>300	16	90	125
CECEC−P_150k	150.5	1.08	0.26	0.24	0.5	2576	>300	13	91	128
$(CECEC)_2$−P_87k	87.3	1.09	0.26	0.25	0.49	1493	<140	19	94	−

[a] Determined from the unsaturated precursors by SEC in THF at 25 °C with polystyrene calibration standards. [b] Calculated using bulk homopolymers densities reported by Fetters et al.[14] with a 118 Å^3 reference volume. [c] Determined by dynamical mechanical spectroscopy. [d] Percent crystallinity in the E blocks determined by DSC. [f] Peak melting temperature of the E blocks determined by DSC.

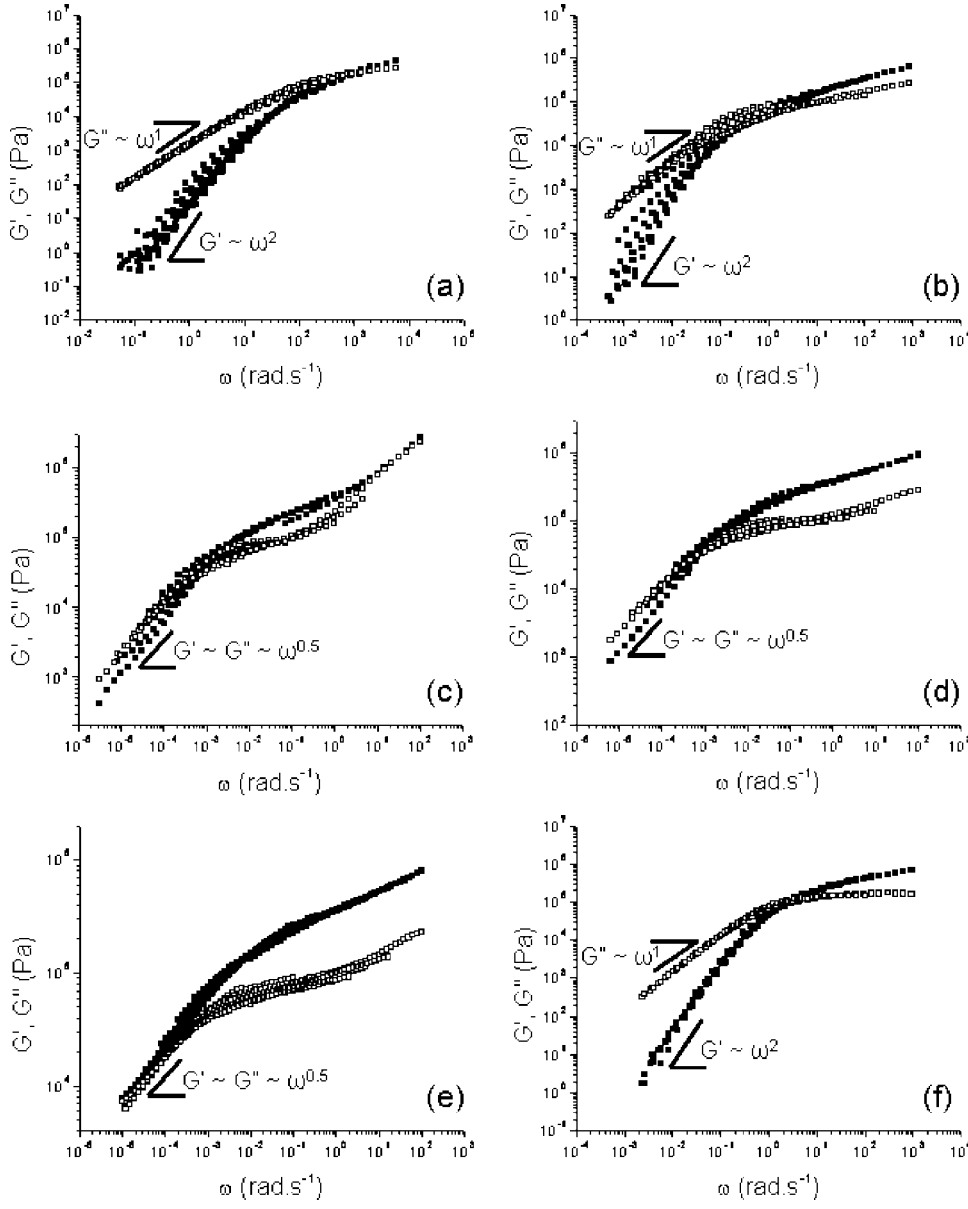

Figure 2. Superposition of isothermal frequency responses to $T_{ref} = 160$ °C for (a) CECEC−P_77k, (b) CECEC−P_85k, (c) CECEC−P_100k, (d) CECEC−P_120k, (e) CECEC−P_150k, and (f) $(CECEC)_2$−P_87k. Open and filled symbols represent G'' and G', respectively.

that the low-frequency elastic ($G' \sim \omega^m$) and loss ($G'' \sim \omega^n$) moduli of a block copolymer are sensitive to the state of order. The disordered liquid state is characterized by $m = 2$ and $n = 1$, while periodic order leads to $m < 1$ and $n < 1$. The low frequency response of samples CECEC−P_77k, CECEC−P_85k and $(CECEC)_2$−P_87k (Figure 2, parts a, b, and f) are consistent with a state of disorder. (Superposition of the terminal portion of the dynamic mechanical spectra in the disordered state is sensitive to the proximity of the material to the ODT. As the ODT is approached the terminal branches of G' and G'' shift to lower frequency while maintaining liquid-like scaling behavior, due to the development of composition fluctuations.[59] This explains why the data for $(CECEC)_2$−P_87k (half the segregation strength of an equal molecular weight hexablock) is better superpositioned than that from CECEC−P_77k and CECEC−P_85k, which are much closer to the ODT.)

Samples CECEC−P_100k, CECEC−P_120k, and CECEC−P_150k are distinctly different with $m = n = {}^1/_2$, consistent with a state of (tentatively lamellar[59]) order.

Small Angle X-ray Scattering. Synchrotron SAXS measurements yielded definitive evidence regarding the state of order, periodic spacing and symmetry of the five CECEC−P hexablock, and single $(CECEC)_2$−P undecablock, copolymers. We have selected representative data obtained at two temperatures, 140 and 250 °C, and presented these results in Figures 3 and 4.

For the hexablock materials the melt state SAXS patterns fall into two broad categories: those exhibiting two relatively broad peaks at both temperatures (Figure 3, parts a and b) and those displaying three or more peaks primarily associated with diffraction from ordered structures (Figure 3c−e). In contrast, the undecablock copolymer produced only one broad peak at both measurement temperatures (Figure 4). These results are evaluated here and considered in the context of the complete set of characterization results in the discussion section.

Each of the peaks found in Figure 3, parts a and b, resembles the well-documented correlation hole scattering found in disordered block copolymers.[15,61] As the combination parameter χN approaches the value associated with the transition from order to disorder ($(\chi N)_{ODT} = 10.5$ within mean field theory for a symmetric diblock copolymer[15]) the peak correlation hole scattering intensity diverges; near the ODT this peak also reflects the effects of composition fluctuations. We interpret the existence of two such peaks in CECEC−P_77k and CECEC−P_85k as the manifestation of two correlation holes, one for the C and E blocks, and another due to CECEC and P. Naturally, these features occur at different q values as a consequence of the larger (P) and smaller (C and E) block molecular weights. Also, the fact that the high- and low-q peaks are of roughly comparable intensity indicates that both types of block correlations reflect roughly similar levels of interactions. This simple analysis indicates that CECEC−P_77k and CECEC−P_85k are disordered over the entire experimental temperature range, a conclusion supported by the mechanical spectroscopy data found in Figure 2, parts a and b.

Increasing the molecular weight of the hexablock copolymers at constant composition leads to qualitative changes in the SAXS patterns. Most dramatic is the development of additional peaks and sharpening of the lowest order reflection in each trace. For the CECEC−P_100k specimen higher order peaks appear at $q/q^* = 2$ ($T = 140$ °C) and 2, 3, and 4 ($T = 250$ °C) as indicated by the arrows in Figure 3c. We interpret these results as evidence of lamellar order between CECEC and P, consistent with the composition and the mechanical spectroscopy data shown in Figure 2c. We are not able to ascertain the state of order between the C and E blocks from these data although the $T = 140$ °C pattern includes a broad peak at $q \cong 0.03$ Å^{-1} that is consistent with correlation hole scattering. At 250 °C, the CECECP-100k hexablock copolymer behaves as a symmetric diblock copolymer where one domain is composed of the mixed CECEC sequences and the other is the P block as underlined by the fairly low intensity of the second order peak consistent with structure factor extinctions for symmetric two-domain lamellae.[62] Further increasing the hexablock molecular weight (CECEC−P_120k and CECEC−P_150k) leads to clear evidence of order in the SAXS data on two length scales as previously reported.[63] Figures 3d and 3e each exhibit a peak at low q and a series of peaks at higher scattering wavevectors, which can be indexed as $q/q^* = 1, 2, 3$ (see arrows). We interpret these results as evidence of two coexisting layered (lamellar) melt structures with length scales d_1^* and d_2^* (see Table 2), where $d^* = 2\pi/q^*$.

Unlike the hexablocks, the $(CECEC)_2$−P_87k undecablock copolymer produced only one relatively broad SAXS peak at all measurement temperatures (see Figure 4), We believe this indicates correlations between molecularly mixed CECEC and P, i.e., analogous to the d_1^* spacing identified with the hexablock melts (see Discussion). (Close inspection of the 140 °C SAXS pattern in Figure 4 suggests the presence of a very weak peak at $q \cong 0.05$ Å^{-1}). Although this polymer has essentially the same overall molecular weight as the disordered material CECEC−P_85k, the equivalent hexablock obtained by splitting the undecablock in half-would be only weakly segregated (i.e., the CECEC blocks in $(CECEC)_2$−P_87k are only half the molecular weight of those in CECEC−P_85k and thus are further from the ODT). Apparently this sufficiently diminishes the electron density contrast within the CECEC sequence to nearly eliminate the associated correlation hole scattering. Here we note that the electron densities of pure E and P melts are virtually identical. Even with a slightly higher carbon content (C_8H_{14} versus CH_2), a significantly higher density leads to a larger electron density for C. If mixed homogeneously we expect E and C to be characterized by an average density and an average electron density greater than that for P. We believe the peaks in Figure 4 reflect pseudo diblock-like correlation hole scattering from homogeneous CECEC and P. (Note, this argument assumes that the development of composition (and hence true density) fluctuations as the ODT is approached produce scattering contrast leading to CECEC correlation hole scattering.)

Two representative SAXS patterns, obtained from CECEC−P_120k at 50 °C and $(CECEC)_2$−P_87k at 80 °C, i.e., below the melting/vitrification temperature, are presented in Figure 5. The scattering pattern from the melt ordered material is nearly indistinguishable from the result at 140 °C (Figure 3d), while E-block crystallization induces the formation of a second, higher q peak for $(CECEC)_2$−P_87k, which we interpret as hierarchical structure.

Transmission Electron Microscopy. Imaging the morphology of the multiblock copolymers was challenging. In order to create electron beam contrast we stained microtomed specimens with RuO_4 for varying amounts of time. Based on our experience with these and other saturated hydrocarbon block copolymers[57,64] P most readily accepts this stain followed by C and then E. Micrographs reflect the morphology of each material at room temperature, following cooling from the melt state, which is accompanied by vitrification of the C domains and crystallization of the E domains, or *vice versa*.

Figure 6 illustrates representative TEM images obtained from the three specimens already shown by SAXS and mechanical spectroscopy to be disordered in the melt state. Hexablocks CECEC−P_77k and CECEC−P_85k are characterized by a disorganized microdomain structure similar in form to a bicontinuous microemulsion. However any definitive assertion cannot be done on the actual bicontinuity of these structures. Undecablock $(CECEC)_2$−P_87k displays a similar pattern but with a smaller length scale. These results are consistent with the development of morphology upon cooling in response to E block crystallization.

Hexablocks CECEC−P_120k and CECEC−P_150k show clear elements of periodic order in all TEM images; CECEC−P_100k was characterized by a microphase-separated morphology with poorly defined order. In Figure 7 we present representative micrographs taken from sample CECEC−P_120k. In order to enhance the degree of long-range order the specimen was sheared using a device described elsewhere.[18] Three different structural motifs were identified in thin slices obtained from this material and are identified in Figure 7. (We were not able to preserve a correlation between the shearing geometry and morphology obtained in the TEM). Combining the three types of micrographs with the doubly periodic layered structure deduced from SAXS (Figure 3d) leads to the morphology sketched in Figure 8, which shows layers of P sandwiched between sheets of microphase-separated CECEC, which cor-

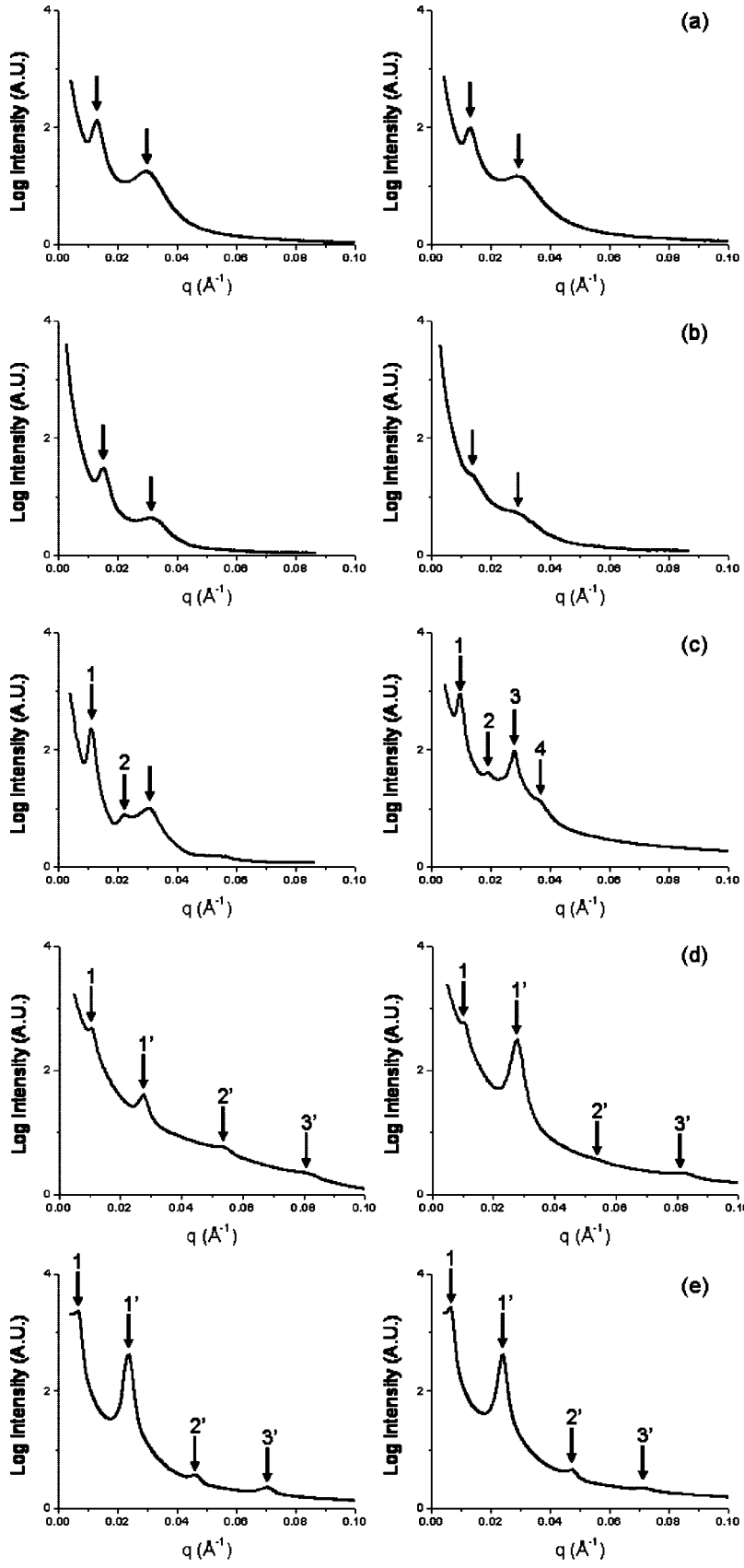

Figure 3. Synchrotron SAXS data acquired at 140 °C (left side) and 250 °C (right side) for (a) CECEC−P_77k, (b) CECEC−P_85k, (c) CECEC−P_100k, (d) CECEC−P_120k and (e) CECEC−P_150k. Arrows identify peak positions. CECEC−P_77k and CECEC−P_85k are disordered and the peaks are associated with correlation hole scattering. CECEC−P_100k is indexed to a singly periodic lamellar morphology while CECEC−P_120k and CECEC−P_150k provide evidence of two lattices with different periodicities.

roborates the morphology reported previously.[63] When the electron beam is directed perpendicular to the P layers (direction *y* in Figure 8) stripes of C and E with overall periodicity d_2* are revealed (Figure 7a). Two different images are obtained in

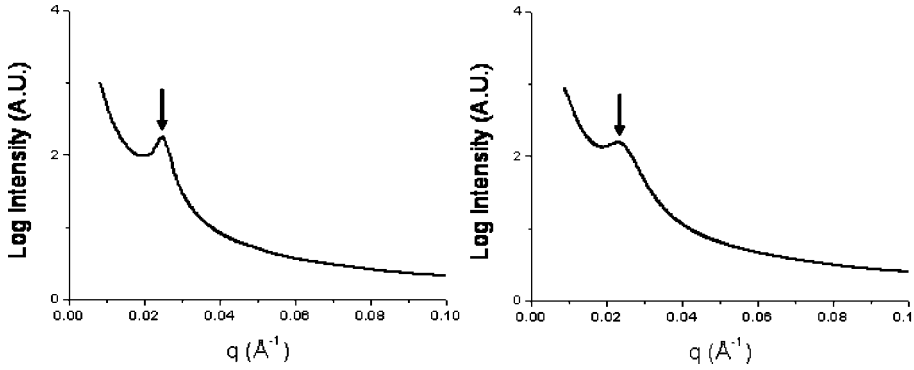

Figure 4. Synchrotron SAXS data acquired at 140 °C (left side) and 250 °C (right side) for $(CECEC)_2$−P_87k.

Table 2. Domain Spacings Calculated from the SAXS Data at 140 ° C for the CECEC−P and $(CECEC)_2$−P Series

sample	q^*_1 (Å^{-1})	d^*_1 (nm)	q^*_2 (Å^{-1})	d^*_2 (nm)	morphology at 140 °C
CECEC−P_77k	0.0129	48.5	0.0295	21.3	Dis[a]
CECEC−P_85k	0.0128	48.9	0.0282	22.2	Dis[a]
CECEC−P_100k	0.0116	54.2	0.0267	23.5	Lam_2[b]
CECEC−P_120k	0.0106	59.0	0.0274	22.8	Lam/Lam[c]
CECEC−P_150k	0.0098	64.1	0.0233	26.9	Lam/Lam[c]
$(CECEC)_2$−P_87k	0.0245	25.6			Dis[a]

[a] Disordered. [b] Two-domain lamellar morphology. [c] Two distinct layered mesostructures.

the limiting cases where the beam is parallel to both the P and the C/E layers (Figure 7b, direction z in Figure 8) and parallel to P but perpendicular to C/E with periodicity d_1* (Figure 7c, direction x in Figure 8). Here we note that the SAXS data from CECEC−P_120k taken above and below the melting/vitrification temperatures (see Figures 3d and 5a) confirms that this morphology is present at all temperatures investigated.

Tensile Mechanical Properties. The mechanical properties of all six multiblock copolymers appearing in Table 1 are summarized in Figure 9. Here engineering stress is plotted versus engineering strain, where tensile tests were conducted up to the point of sample rupture. We must emphasize that in all cases the test specimens failed at the grip indicating that the reported stresses and strains at break represent lower limits. Numerical values of the elastic modulus (E), yield stress, stress at break, and strain at break are listed in Table 3.

With one exception the materials examined display a similar elastic modulus, E = 20−30 MPa. (On the basis of an entanglement molecular weight of $M_{e,P}$ = 1,6 kg·mol^{-1}, rubbery P should have a room temperature modulus of E_P = 4 MPa, which is a small fraction of the values listed in Table 3.) We attribute the higher modulus for sample CECEC−P_100k to a moderately higher glass content ($E_C \cong$ 3000 MPa[12]) and to a possibly modified or oriented morphology that presents slightly more glassy C material to the mechanical measurement. Yield stress levels follow the same trend. Values for the strain at break fall into two categories: the disordered hexablocks (∼750%), and the ordered hexablocks and the undecablock (∼1500%). The stress at break can be crudely group into three categories: disordered hexablocks (∼5 MPa), ordered hexablocks (10−20 MPa), and the undecablock (32 MPa). All the materials are considered to be rather tough and resilient although the differences we report are significant and worthy of further consideration (see Discussion).

Cyclic tensile tests (loading and unloading) were performed on all the multiblock materials. Representative sets of stress versus strain curves for CECEC−P_120k, and $(CECEC)_2$−P_87k are presented in Figure 10. For clarity, only the first, second, and sixth cycles are shown along with the final extension to rupture. We have extracted two properties from these data. Initial elastic strain recovery is defined as the maximum applied strain (600% in Figure 10) minus the strain for which the point of zero stress upon unloading during the first cycle is achieved (vertical arrows in Figure 10). The permanent set is the nonrecoverable strain defined here as the strain at which a measurable stress is recorded during subsequent extension (see dashed lines in Figure 10a,b).

In all cases examined, the stress−strain behavior of the first cycle was substantially different from subsequent cycles, which were all highly reproducible. This is commonly found with thermoplastic elastomers and attributed to the impact of thermomechanical history on chain conformation and crystallite distribution. After the initial cycle, CECEC−P hexablock copolymers and the $(CECEC)_2$−P undecablock copolymer exhibit a low degree of strain softening and a highly elastic response during the second through sixth cyclic loading experiments. The initial elastic strain recovery and the permanent sets after the first and the sixth cycles are summarized for each multiblock copolymer in Table 4. The initial elastic strain recovery is relatively invariant (∼2.5) for the hexablock copolymers while the $(CECEC)_2$−P_87k undecablock copolymer exhibits a significantly greater initial recovery of elastic strain (∼4.5) demonstrating the influence of molecular architecture on this mechanical property.

Discussion

A series of six CECEC−P hexablock copolymers, and one $(CECEC)_2$−P undecablock copolymer, were synthesized using a combination of sequential anionic polymerization and catalytic hydrogenation leading to relatively low polydispersity (M_w/M_n < 1.1) products. These materials combine glassy (C), semicrystalline (E), and rubbery (P) polymers through molecular architectures that self-assemble into hierarchical mesostructures that impart useful mechanical properties. The CECEC pentablock portion of the molecules leads to relatively stiff, mechanically robust domains while the rubbery P block adds energy dissipative and compliant domains. We designed these compounds in order to assess whether these viscoelastic elements could be combined without the loss of toughness and extensibility. In the course of this work we have discovered a new hierarchical morphology, and established that the CECEC pentablock architecture produces tough microdomains when cooled from either the segregated or homogeneous states. This section discusses our findings in the context of current theory and prior experimental reports.

Phase Behavior and Morphology. As deduced from the SAXS and rheological analyses, CECEC−P_77k and CECEC−P_85k are disordered in the melt state, i.e. T_{ODT} is below either the glass transition or crystallization temperatures. However the TEM micrographs presented in pats a and b of Figure 6 clearly

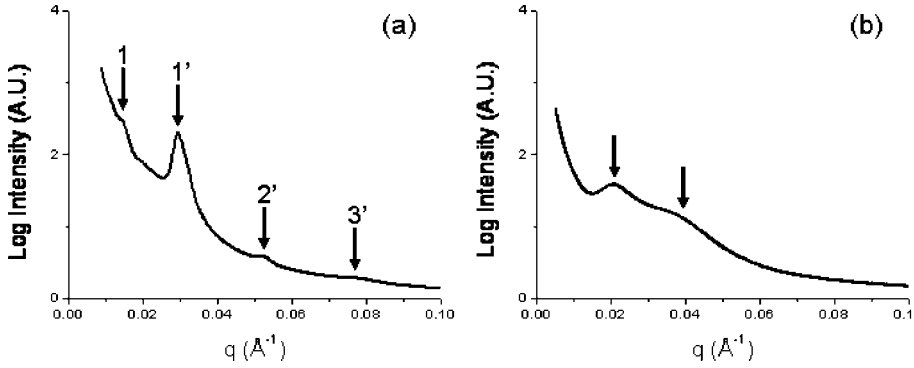

Figure 5. Synchrotron SAXS data acquired for (a) CECEC−P_120k at 50 °C and (b) for $(CECEC)_2$−P_87k at 80 °C.

show a heterogeneous state at room temperature. We believe that segregation is induced in these materials from the homogeneous disordered melt by crystallization of the E blocks[65−68] with the attendant expulsion of C and P from the E domains. However "direct" crystallization induced segregation (which would produce much smaller domains and a structure similar to the one found in Figure 6c) is not the only process involved in the formation of the mesostructure shown in Figure 6a,b. The room temperature morphology for CECEC−P_77k and CECEC−P_85k is the result of two processes: partial crystallization of the E blocks, which forces segregation of the adjacent C blocks, and subsequent ejection of the longer P blocks on a larger length scale. The resulting morphology appears to be a bicontinuous structure with a characteristic spacing $d_1^* \approx 49$ nm that agrees with the larger correlation hole spacing recorded at 140 °C by SAXS (Table 2). Based on our experience with RuO_4, E, C, and P will appear light, gray, and black, respectively, in TEM images. Therefore, we associate the gray and black regions in Figure 6a and b with disordered but segregated CECEC dispersed in P. Because these structures are not ordered, identification of smaller individual E and C domains is difficult. Nevertheless, small (ca. 5 nm) white objects, which we believe are E crystals, can be found throughout these images. The relative projected areas of gray and black in the TEM images are consistent with the composition of the hexablocks (50% CECEC and 50% P), and this composition is also most conducive to the formation of a bicontinuous structure.

These observations also apply in part to $(CECEC)_2$−P_87k, which has roughly half the segregation strength of the two disordered hexablock materials, which may influence the nucleation and grown rates of the E blocks, However, the most important factor responsible for the much finer morphology evident in Figure 6c is the reduction by one-half of the C, E, and P block molecular weights relative to CECEC−P_85k.

On the basis of SAXS and rheological analyses, CECEC−P_100k, CECEC−P_120k and CECEC−P_150k adopt a microphase-separated lamellar structure in the melt. The morphology documented by TEM for CECEC−P_100k at room temperature (not shown) appears to be less well ordered than that found for CECEC−P_120k and _150k. We again attribute this behavior to the effects of crystallization during cooling, which likely disrupt the relatively weakly segregated lamellar phase present at elevated temperatures. Such structural disruption was not encountered with CECEC−P_120k or CECEC−P_150k as illustrated in Figure 7, which provides evidence for a new type of hierarchical lamellar mesostructure with a double periodicity as documented in a previous publication.[63] Rationalization on both enthalpic and entropic grounds of this hierarchical perpendicular lamellae in parallel lamellae mesostructure depicted in Figure 8 have been reported elsewhere.[63]

Quantitative estimates of the temperature-dependent interaction parameters for all three combinations of C, E, and P have been reported by our group, where $\chi_{CE}(T) > \chi_{CP}(T) \gg \chi_{EP}(T)$.[69−71] Chain connectivity in the CECEC−P sequence forces contact between C and E, and C and P, segments, while the interactions between E and P blocks are the most favorable. Above a threshold molecular weight the CECEC portion of the hexablock will microphase separate. (Pure CECEC containing equal volume fractions of E and C order above about $M_n = 50$ kg·mol^{-1} at roughly 195 °C[72]). Below this threshold value disordered CECEC is expected to mix with the P block since this dilutes C/E contacts in exchange for more favorable C/P and E/P contacts. We believe this explains the completely disordered melt state in CECEC−P_77k, CECEC−P_85k, and $(CECEC)_2$−P_87k.

Remarkably, increasing the hexablock molecular weight from 85 to 100 kg/mol at constant composition results in a massive increase in the order−disorder transition temperature, from T_{ODT} < 140 °C to T_{ODT} > 300 °C (Table 1). We do not have a convincing explanation for this surprising result, a phenomenon that is under active investigation in our laboratory. (We have discovered similar behavior in other multiblock copolymers containing C, E, and P).[73] Saturated hydrocarbons are governed by rather simple van der Waals interactions and it is tempting to assume well-behaved pair wise χ parameters for binary mixtures of polyolefins. In fact, when modeled as $\chi = AT^{-1} + B$, the relative magnitude of constants A and B vary considerably among pairs of polyolefins. One explanation for this effect is that the relatively weak enthalpic segment−segment interactions can be overwhelmed by entropically based packing nonidealities. Block copolymers containing three different types of saturated hydrocarbon blocks, such as C, E, and P, are likely to be even more complicated. Each block may have a different thermal expansion coefficient, and a different segmental shape. How these factors combine to determine T_{ODT} is impossible to predict at this time.

Figure 11 shows the domain spacings, d_1^* and d_2^*, and the ratio d_2^*/d_1^* obtained from the SAXS data at 140 °C, plotted versus the degree of polymerization N_0 of the CECEC−P and the CECEC sequences, respectively; N_0 is defined based on a segment volume of 118 Å^3. These domain spacings scale as $d_1^* \sim N_o^{0.45\pm0.03}$ and $d_2^* \sim N_o^{0.33\pm0.05}$, surprisingly small scaling exponents when compared to the behavior of simple linear block copolymers, $d \sim N_0^{1/2}$ and $d \sim N_0^{2/3}$ in the limits of weak[61] and strong[74−77] segregation, respectively. At least two factors may contribute to this behavior. First, the specimens under consideration span the order−disorder transition and the apparent scaling relationships reflect in part the transition between these limits. Second, the scaling exponents will be directly influenced by the coupling between order in the CECEC substructure (domain spacing d_2^*) and between this ordered substructure and the P domains (domain spacing d_1^*). However, we do not understand how these competing constraints result in the observed small scaling exponents, and look forward to gaining

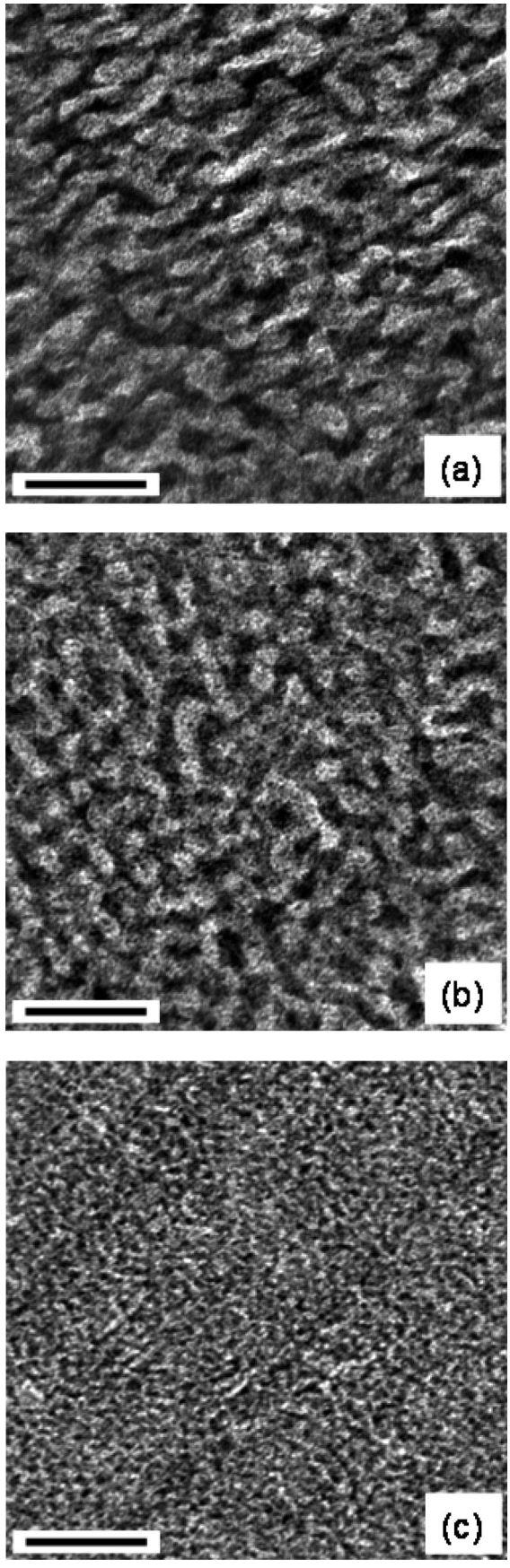

Figure 6. TEM micrographs of the (a) CECEC−P_77k, (b) CECEC−P_85k and (c) $(CECEC)_2$−P_87k undecablock copolymer. Dark regions in the TEM micrographs result from RuO_4 staining of the P domains. The weakly stained C and E appear much lighter. Scale bars correspond to 100 nm.

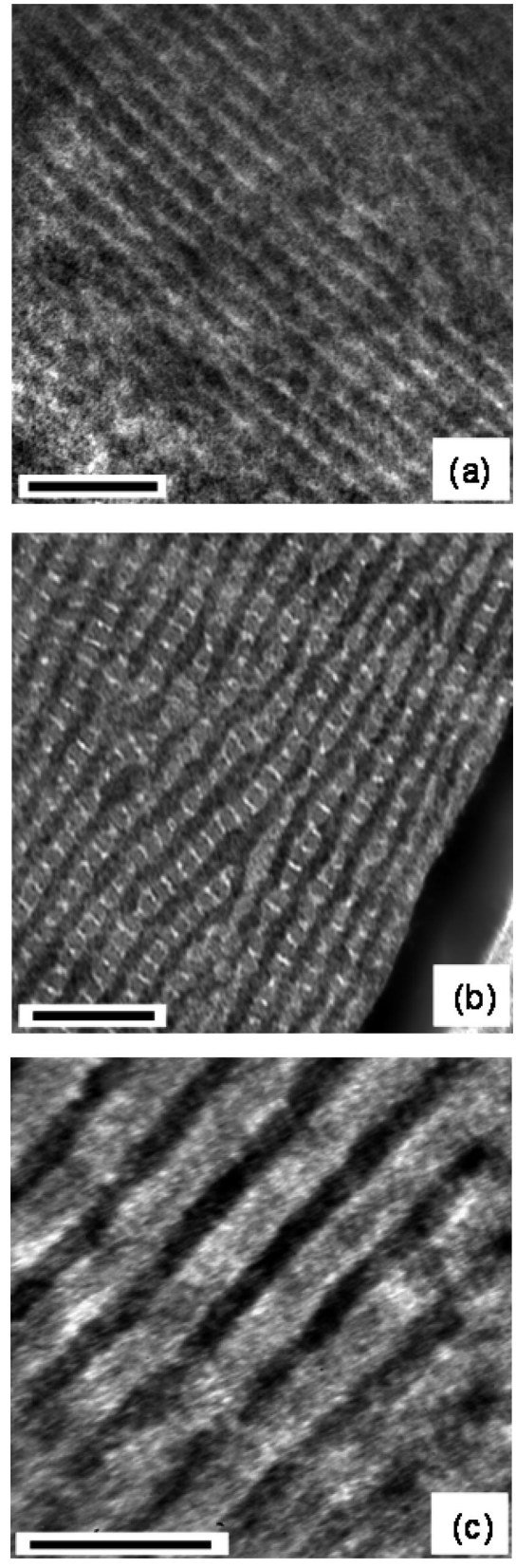

Figure 7. TEM micrographs obtained from different RuO_4 stained thin sections of CECEC−P_120k. Scale bars correspond to 100 nm. These images are associated with three orthogonal projections of the doubly lamellar morphology illustrated in Figure 8. (a) Gray and white stripes are interpreted as C and E, respectively, representing the $x-z$ projection in Figure 8. (b) White, gray, and black domains are attributed to E, C, and P domains, respectively, representing the $x-y$ projection in Figure 8. (c) Gray and black layers are assigned to C/E and P respectively, a projection onto the $y-z$ plane in Figure 8.

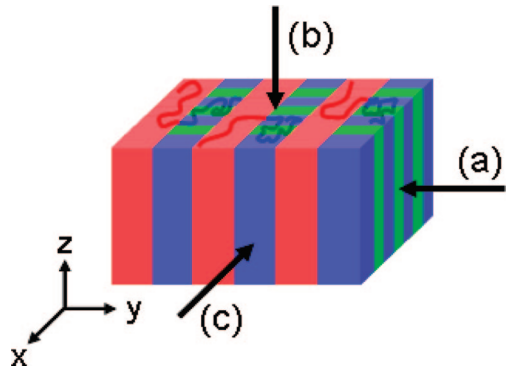

Figure 8. Schematic representation of the hierarchical perpendicular lamellar mesostructure deduced from SAXS and TEM results. The three arrows are associated with the three corresponding TEM micrographs of the doubly lamellar morphology shown in Figure 7. Domains correspond to P (red) = poly(ethylene-*alt*-propylene), C (blue) = poly(cyclohexylethylene), and E (green) = poly(ethylene).

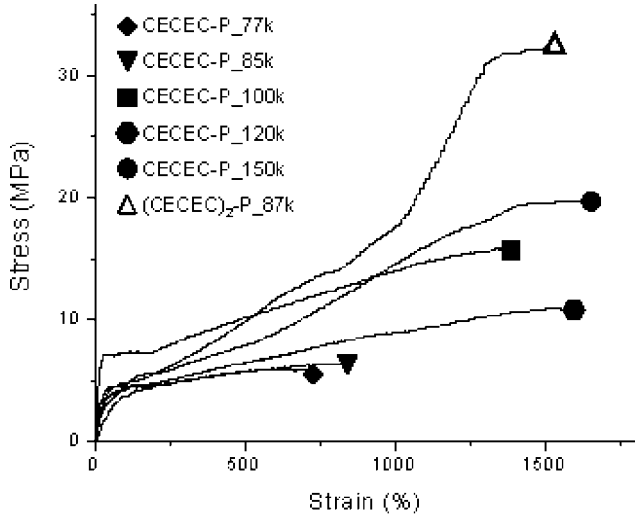

Figure 9. Representative engineering stress versus stain curves for CECEC−P hexablock copolymers and $(CECEC)_2$−P undecablock copolymer.

Table 3. Mechanical Properties of CECEC−P and $(CECEC)_2$−P Block Copolymers

Sample	E (MPa)	yield stress (MPa)	strain at break	stress at break (MPa)
CECEC−P_77k	22 ± 2	4.4 ± 0.5	6.8 ± 0.6	5.2 ± 0.6
CECEC−P_85k	21 ± 2	4.7 ± 0.6	8.1 ± 0.9	5.6 ± 0.4
CECEC−P_100k	72 ± 6	7 ± 0.7	13.5 ± 0.5	15.5 ± 1
CECEC−P_120k	25 ± 4	5.5 ± 1	15.2 ± 0.8	10.6 ± 1.5
CECEC−P_150k	24 ± 3	5.7 ± 0.4	16.2 ± 1.2	18.8 ± 2.3
$(CECEC)_2$−P_87k	28 ± 5	5.2 ± 0.6	15.9 ± 0.9	31.8 ± 4.7

additional insights by conducting SCFT calculations. As a result the apparent invariance in d_2^*/d_1^* with molecular weight may be a manifestation of such coupling (a least-squares fit would result in $d_2^*/d_1^* \sim N^{-0.12\pm0.06}$).

Curiously, the spacing determined for $(CECEC)_2$−P_87k is well below the extrapolated d_1^* curve when N_0 is taken to be half the overall undecablock length. We attribute this phenomenon to the presence of an unique correlation hole scattering peak for the whole $(CECEC)_2$−P sequence and by the large-amplitude compositional fluctuations inherent to systems with low segregation strength.[61]

Mechanical Properties. The CECEC−P hexablock copolymers display a compliment of interesting and potentially useful mechanical properties, which we consider in this section. All

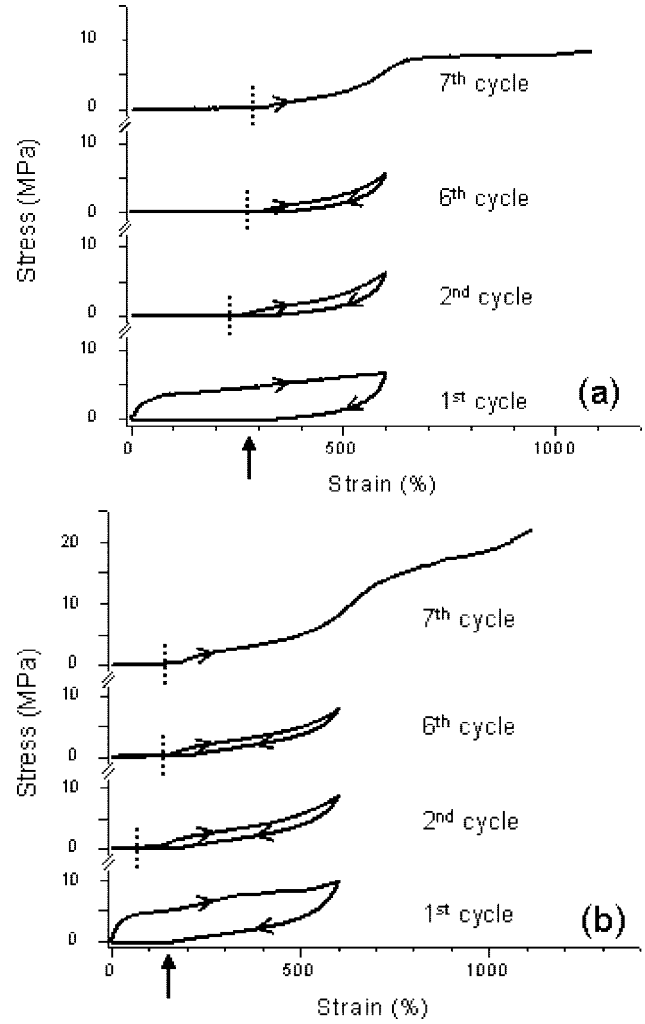

Figure 10. Representative cyclic loading and unloading behavior for (a) CECEC−P_120k and (b) $(CECEC)_2$−P_87k. Arrows identify the point of zero stress during strain recovery in the first cycle while dashed lines identify the point of nonzero stress during extension in the second, sixth, and seventh cycles.

Table 4. Mechanical Properties of CECEC−P Block Copolymers under Cyclic Loading and Unloading

sample	initial elastic strain recovery[a]	permanent set[b] (after the first cycle/ after the sixth cycle)	strain at break
CECEC−P_77k	2	2.1/2.6	5.9
CECEC−P_85k	2.1	2/2.5	7.1
CECEC−P_100k	2.4	2.5/3.1	11.8
CECEC−P_120k	2.8	2.3/2.9	10.8
CECEC−P_150k	2.7	2.1/2.6	12.7
$(CECEC)_2$−P_87k	4.5	0.7/1.5	11.1

[a] Defined as the maximum applied strain minus the strain for which the point of zero stress upon unloading during the first cycle is achieved (vertical arrows in Figure 10). [b] Nonrecoverable strain defined here as the strain at which a measurable stress is recorded during subsequent extension (see dashed lines in Figure 10a,b).

the specimens, except one, have a common elastic Young's modulus, $E = 21 - 25$ MPa; the modulus for CECEC−P_100k is significantly higher, $E = 72$ MPa, attributable to a modestly greater glass content (see Table 1). A nearly invariant modulus is consistent with comparable states of microdomain continuity between specimens, notwithstanding differences in the states of order. Assuming the modulus E is dominated by the CECEC portion of the microstructure, the bicontinuous and polydomain lamellar morphologies present equivalent average structural continuity. This argument also holds for the $(CECEC)_2$−P_87k

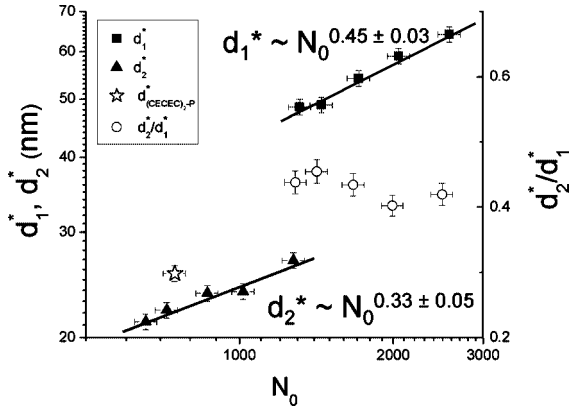

Figure 11. Domain spacings d_1* and d_2*, and d_2*/d_1* versus degree of polymerization N_0 for CECEC−P hexablock copolymers. N_0 for d_1* corresponds to the overall CECEC−P sequence, while N_0 for d_2* refers to the CECEC sequence.

undecablock copolymers, for which $E = 28$ MPa. For similar reasons, a second important property, the yield stress, also is nearly invariant across all the multiblock materials ($4.4 \leq \sigma_y \leq 5.7$ MPa) with the exception of CECEC−P_100k ($\sigma_y = 7$ MPa).

Once these polymers yield, the stress−strain response varies depending upon the molecular architecture and the morphology.[68,78,79] Clear differences distinguish the nonlinear mechanical behavior of CECEC−P_77k and CECEC−P_85k from CECEC−P_100k, CECEC−P_120k, and CECEC−P_150k. The disorganized, bicontinuous-like morphology present at the two lowest molecular weights is accompanied by half the strain at break and a third to a half of the stress at break produced by the hierarchical lamellar structure (see Table 3 and Figure 9). Based on these data alone, we can not determine whether these differences result from variations in the structure and inherent strength of the CECEC subdomains, or the collective response of the entire morphologies. The undecablock was prepared specifically to help us discriminate between these and other possible mechanisms.

Sample $(CECEC)_2$−P_87k was designed to be disordered at all temperatures above the melting point of the E blocks, a criterion ensured by the combination of molecular weight and architecture. Despite a lower CECEC molecular weight ($M_{n,CECEC} = 22$ kg·mol^{-1}) this material displays a similar level of crystallinity as the hexablock copolymers ($M_{n,CECEC} \geq 39$ kg·mol^{-1}, see Table 1). Hence, upon cooling from an elevated temperature, partial crystallization of the E blocks drives microphase separation of E, C, and P, with subsequent vitrification of C as the material is cooled to room temperature. We do not know the local arrangement of E and C microdomains in this material. (Nor do we know the local configuration of C and E at room temperature in the two hexablocks prepared from the disordered state.) Nevertheless, the placement of CECEC pentablocks at either end of the central P block results in a remarkably tough, strong and resilient material.[78−81] An unanticipated outcome of this work is the discovery that weakly segregated CECEC pentablock copolymer forms remarkably strong nanoscale domains when induced to order through crystallization of the E blocks.

Comparison of the stress and strain at break for CECEC−P_77k and CECEC−P_85k with $(CECEC)_2$−P_87k indicates that the intrinsic strength of the CECEC subunits does not limit for the poorer performance of the hexablocks. We believe the disordered bicontinuous morphology of the lower molecular weight hexablocks is less easily rearranged than the doubly lamellar structure (Figure 8) at higher molecular weights, leading to greater strain softening and rupture at smaller strains. Apparently, the two-dimensional CECEC sheets have superior cohesion and must be able to slide past each other owing to the lubricating action of the liquid-like P layers. (Based on these results we speculate that it may be possible to obtain large individual sheets of the CECEC−P hexablock materials by swelling the ordered doubly lamellar polymer with a solvent selective for P). In all cases the P blocks are well above the entanglement molecular weight, which should introduce a time dependence to this relaxation mechanism; we intend to examine this feature in the future. Also, combining the reinforcement of the undecablock architecture and the reinforced layered lamellar morphology may result in a product with an even great breaking stress while retaining a large (∼1500%) ultimate strain.

The performance of the undecablock copolymer compares favorably with the $(EP)_n$ multiblock materials described earlier.[79] Asymptotic $(EP)_n$ properties of 900% strain at break and 30 MPa strength require either strong segregation ($M_n > 250$ kg·mol^{-1}) or more than eight disordered blocks ($n > 8$). Either criterion leads to high melt viscosities owing to the very low entanglement molecular weight of E ($M_{e,E} \approx 800$ g·mol^{-1}) and P ($M_{e,P} \approx 1600$ g·mol^{-1}). $(CECEC)_2$−P_87k has a 50% greater strain at break, a slightly higher ultimate strength, and a much lower melt viscosity due to a lower overall molecular weight and the incorporation of C segments ($M_{e,C} \approx 40000$ g·mol^{-1}). Moreover, the three different mechanical building blocks (glassy C, semicrystalline E, and rubbery P) provide almost unlimited latitude for tailoring the mechanical response between rubbery and plastic.[73,81−83]

Cyclic loading and unloading tests provide additional insight into the mechanisms controlling the stress−strain response of these multiblock copolymers. Two data sets are shown in Figure 10, representing the hexablocks and the undecablock. Here, 48% of the 600% strain initially imposed (first cycle) on sample CECEC−P_120k was recovered when the sample was unloaded. Similar responses were obtained with the other hexablock copolymers (see Table 4). $(CECEC)_2$−P_87k performed significantly better with 75% recovery of the applied strain after the initial deformation. We interpret these results as evidence of more permanent shearing in the hexablocks, due to the loose and rubbery P blocks, versus reversible stretching of the doubly fixed P blocks in the undecablock. Subsequently, all samples respond rather elastically between specimen lengths established at the initial point of unloading and the maximum strain of 600% (or 500%). After six cycles, the polymers were strained to rupture. As shown in Figure 10, beyond the maximum cyclic strain the stress registered by the hexablock remains almost constant (strain softening) while the undecablock stress increases up to the point of failure. These results are consistent with our speculation regarding internal shearing of the singly attached P blocks versus stretching of the doubly tethered P blocks. In both cases, we believe the CECEC domains remain intact and provide the strength responsible for sample integrity.

Conclusion

A series of five CECEC−P hexablock copolymers, and one $(CECEC)_2$−P undecablock copolymer were prepared with molecular weights ranging from 77 to 150 kg·mol^{-1} and containing 50% P, 25% E and 25% C. The phase behavior and mechanical properties have been investigated by small-angle X-ray scattering, transmission electron microscopy, and tensile testing. High molecular weight CECEC−P microphase separates in the melt state into a hierarchical mesostructure with strips of C and E forming layers arranged in alternating lamellar form with P. This morphology persists at lower temperatures following partial crystallization of the E blocks and vitrification of C. Low molecular weight, melt disordered, CECEC−P and $(CECEC)_2$−P undergo crystallization-induced microphase sepa-

ration upon cooling resulting in a disordered bicontinuous structure with poor long-range order. The mechanical properties of these materials depend on the mode of segregation and the molecular architecture. Remarkably high failure stress and rupture strain were obtained from the undecablock copolymer material, demonstrating the intrinsic toughness of the microphase-separated CECEC domains, even when grown from a weakly segregated homogeneous state. Cyclic tensile tests also reflect the response of singly and doubly tethered P block in CECEC−P and $(CECEC)_2$−P.

Acknowledgment. The authors gratefully acknowledge financial support from the National Science Foundation (DMR-0220460). Portions of this work were carried out in the University of Minnesota Institute of Technology Characterization Facility, which receives partial support from NSF through the NNIN program and the Materials Research Science and Engineering Center (NSF-MRSEC) at the University of Minnesota (NSF DMR-0212302). Work performed at the DuPont−Northwestern−Dow Collaborative Access Team (DNDCAT) located at Sector 5 of the Advanced Photon Source (APS). DND−CAT is supported by E. I. du Pont de Nemours & Co., The Dow Chemical Company, and the State of Illinois. Use of the Advanced Photon Source (APS) was supported by the U.S. Department of Energy, Office of Science, Office of Basic Energy Sciences, under Contract DE-AC02-06CH11357.

Supporting Information Available: Figures showing ^{1}H NMR spectra of SBSBS−I_120k and CECEC−P_120k. This material is available free of charge via the Internet at http://pubs.acs.org.

References and Notes

(1) Holden, G.; Legge, N. R.; Quirk, P. R.; Schroeder, H. E., *Eds. Thermoplastic Elastomers*, 2nd ed.; Hanser Publishers: New York, 1996.
(2) Bates, F. S. *Science* **1991**, *251*, 898–905.
(3) Lodge, T. P. *Macromol. Chem. Phys.* **2003**, *204*, 265–273.
(4) Séguéla, R.; Prud'homme, J. *Macromolecules* **1981**, *14*, 197–202.
(5) Pakula, T.; Saijo, K.; kawai, H.; Hashimoto, T. *Macromolecules* **1985**, *18*, 1294–1302.
(6) Morton, M.; McGrath, J. E.; Juliano, P. C. *J. Polym. Sci., Part C* **1969**, *26*, 99–115.
(7) Holden, G.; Bishop, E. T.; Legge, N. *R J. Polym. Sci., Part C* **1969**, *26*, 37–57.
(8) Honeker, C. C.; Thomas, E. L. *Chem. Matter.* **1996**, *8*, 1702–1714.
(9) Cohen, Y.; Albalak, R. J.; Dair, B. J.; Capel, M. S.; Thomas, E. L. *Macromolecules* **2000**, *33*, 6502–6516.
(10) Cohen, Y.; Thomas, E. L. *Macromolecules* **2003**, *36*, 5265–5270.
(11) Bates, F. S.; Fredrickson, G. H.; Hucul, D. A.; Hahn, S. F. *AlChE J.* **2001**, *47*, 762–765.
(12) Hucul, D. A.; Hahn, S. F. *Adv. Matter.* **2000**, *12*, 1855–1858.
(13) Zhao, J.; Hahn, S. F.; Hucul, D. A.; Meunier, D. M. *Macromolecules* **2001**, *34*, 1737–1741.
(14) Fetters, L. J.; Lohse, D. J.; Richter, D.; Witten, T. A.; Zirkel, A. *Macromolecules* **1994**, *27*, 4639–4647.
(15) Leibler, L. *Macromolecules* **1980**, *13*, 1602–1617.
(16) Bates, F. S.; Fredrickson, G. H. *Annu. Rev. Phys. Chem.* **1990**, *41*, 525–557.
(17) Khandpur, A. K.; Förster, S.; Bates, F. S.; Hamley, I. W.; Ryan, A. J.; Bras, W.; Almdal, K.; Mortensen, K. *Macromolecules* **1995**, *28*, 8796–8806.
(18) Koppi, K. A. *Ph.D. Thesis*; Department of Chemical Engineering and Materials Science, University of Minnesota: Minneapolis, MN, **1993**.
(19) Cochran, E. W.; Garcia-Cervera, C. J.; Fredrickson, G. H. *Macromolecules* **2006**, *39*, 2449–2451.
(20) Bates, F. S.; Fredrickson, G. H. *Phys. Today* **1999**, *52*, 32–38.
(21) Helfand, E.; Wasserman, Z. R. *Macromolecules* **1976**, *9*, 879–888.
(22) Gehlsen, M. D.; Almdal, K.; Bates, F. S. *Macromolecules* **1992**, *25*, 939–943.
(23) Adams, J. L.; Graessley, W. W.; Register, R. A. *Macromolecules* **1994**, *27*, 6026–6032.
(24) Matsushita, Y.; Nomura, M.; Watanabe, J.; Mogi, Y.; Noda, I.; Imai, M. *Macromolecules* **1995**, *28*, 6007–6013.
(25) Ryu, C. Y.; Lee, M. S.; Hajduk, D. A.; Lodge, T. P. *J. Polym. Sci., Part B* **1997**, *35*, 2811–2823.
(26) Matsen, M. W.; Thompson, R. B. *J. Chem. Phys.* **1999**, *111*, 7139–7146.
(27) Tyler, C. A.; Morse, D. C. *Phys. Rev. Lett.* **2005**, *94*, 208302.
(28) Bailey, T. S.; Hardy, C. M.; Epps, T. H., III.; Bates, F. S. *Macromolecules* **2002**, *35*, 7007–7017.
(29) Epps, T. H., III.; Cochran, E. W.; Hardy, C. M.; Bailey, T. S.; Waletzko, R. S.; Bates, F. S. *Macromolecules* **2004**, *37*, 7085–7088.
(30) Epps, T. H., III.; Cochran, E. W.; Bailey, T. S.; Waletzko, R. S.; Hardy, C. M.; Bates, F. S. *Macromolecules* **2004**, *37*, 8325–8341.
(31) Matsushita, Y.; Takasu, T.; Yagi, K.; Tomioka, K.; Noda, I. *Polymer* **1994**, *35*, 2862–2866.
(32) Vigild, M. E.; Chu, C.; Sugiyama, M.; Chaffin, K. A.; Bates, F. S. *Macromolecules* **2001**, *34*, 951–964.
(33) Hermel, T. J.; Wu, L.; Hahn, S. F.; Lodge, T. P.; Bates, F. S. *Macromolecules* **2002**, *35*, 4685–4689.
(34) Wu, L.; Lodge, T. P.; Bates, F. S. *Macromolecules* **2004**, *37*, 8184–8187.
(35) Matsushita, Y.; Mogi, Y.; Mukai, H.; Watanabe, J.; Noda, I. *Polymer* **1994**, *35*, 246–249.
(36) Goldacker, T.; Abetz, V.; Stadler, R.; Erukhimovich, L.; Leibler, L. *Nature (London)* **1999**, *398*, 137–139.
(37) Goldacker, T.; Abetz, V. *Macromol. Rapid Commun.* **1999**, *20*, 415–418.
(38) Abetz, V.; Goldacker, T. *Macromol. Rapid Commun.* **2000**, *21*, 16–34.
(39) Erukhimovich, I.; Smirnova, Y. G.; Abetz, V. *J. Polym. Sci., Ser. A* **2005**, *45*, 1093–1105.
(40) Ruokolainen, J.; Mäkinen, R.; Torkkeli, M.; Mäkelä, T.; Serimaa, R.; ten Brinke, G.; Ikkala, O. *Science* **1998**, *280*, 557–560.
(41) Ruokolainen, J.; ten Brinke, G.; Ikkala, O. *Adv. Mater.* **1999**, *11*, 777–780.
(42) Ikkala, O.; ten Brinke, G. *Science* **2002**, *295*, 2407–2409.
(43) Nandan, B.; Lee, C.-H.; Chen, H.-L.; Chen, W.-C. *Macromolecules* **2006**, *39*, 4460–4468.
(44) Chiang, W.-S.; Lin, C.-H.; Nandan, B.; Yeh, C.-L.; Rahman, M. H.; Chen, W.-C.; Chen, H.-L. *Macromolecules* **2008**, *41*, 8138–8147.
(45) Nagata, Y.; Masuda, J.; Noro, A.; Cho, D.; Takano, A.; Matsushita, Y. *Macromolecules* **2005**, *38*, 10220–10225.
(46) Masuda, J.; Takano, A.; Nagata, Y.; Noro, A.; Matsushita, Y. *Phys. Rev. Lett.* **2006**, *97*, 098301.
(47) Matsushita, Y. *Polym. J.* **2008**, *40*, 177–183.
(48) Nap, R. J.; Kok, C.; ten Brinke, G.; Kuchanov, S. I. *Eur. Phys. J. E* **2001**, *4*, 515–519.
(49) Nap, R.; Erukhimovich, I.; ten Brinke, G. *Macromolecules* **2004**, *37*, 4296–4303.
(50) Nap, R.; Sushko, N.; Erukhimovich, I.; ten Brinke, G. *Macromolecules* **2004**, *37*, 4296–4303.
(51) Subbotin, A.; Klymko, T.; ten Brinke, G. *Macromolecules* **2007**, 2915–2918.
(52) Smirnova, Y. G.; ten Brinke, G.; Erukhimovich, I. *J. Chem. Phys.* **2006**, *124*, 054907.
(53) Kriskin, Y. A.; Erukhimovich, I. Ya.; Khalatur, P. G.; Smirnova, Y. G.; ten Brinke, G. *J. Chem. Phys.* **2008**, *128*, 244903.
(54) Li, W.; Shi, A.-C. *Macromolecules* **2009**, *42*, 811–819.
(55) Ndoni, S.; Papadakis, C. M.; Bates, F. S.; Almdal, K. *Rev. Sci. Instrum.* **1995**, *66*, 1090–1095.
(56) Bandrup, J.; Immergut, E. H. *Polymer Handbook*, 3rd ed.; John Wiley & Sons: New York, 1989.
(57) Khandpur, A.; Macosko, C. W.; Bates, F. S. *J. Polym. Sci., Polym. Phys.* **1995**, *33*, 247–252.
(58) Hillmyer, M. A.; Bates, F. S. *Macromolecules* **1996**, *29*, 6994–7002.
(59) Rosedale, J. H.; Bates, F. S. *Macromolecules* **1990**, *23*, 2329–2338.
(60) Kossuth, M. B.; Morse, D. C.; Bates, F. S. *J. Rheol.* **1999**, *43*, 167–192.
(61) Almdal, K.; Rosedale, J. H.; Bates, F. S.; Wignall, G. D.; Fredrickson, G. H. *Phys. Rev. Lett.* **1990**, *65*, 1112–1115.
(62) Epps, T. H., III.; Cochran, E. W.; Bailey, T. S.; Waletzko, R. S.; Hardy, C. M.; Bates, F. S. *Macromolecules* **2004**, *37*, 8325–8341.
(63) Fleury, G.; Bates, F. S. *Macromolecules* **2009**, *42*, 1691–1694.
(64) Hermel, T. J.; Hahn, S. F.; Chaffin, K. A.; Gerberich, W. W.; Bates, F. S. *Macromolecules* **2003**, *36*, 2190–2193.
(65) Cohen, R. E.; Cheng, P. L.; Douzinas, K.; Kofinas, P.; Berney, C. V. *Macromolecules* **1990**, *23*, 324–327.
(66) Séguéla, R.; Prud'homme, J. *Polymer* **1989**, *30*, 1446–1455.
(67) Rangarajan, P.; Register, R. A.; Fetters, L. J. *Macromolecules* **1993**, *26*, 4640–4645.
(68) Koo, C. M.; Wu, L.; Lim, L. S.; Mahanthappa, M. K.; Hillmyer, M. A.; Bates, F. S. *Macromolecules* **2005**, *38*, 6090–6098.
(69) Cochran, E. W.; Bates, F. S. *Macromolecules* **2002**, *35*, 7368–7374.
(70) Rosedale, J. H.; Bates, F. S.; Almdal, K.; Mortensen, K.; Wignall, G. D. *Macromolecules* **1995**, *28*, 1429–1443.

(71) Maurer, W. W.; Bates, F. S.; Lodge, T. P.; Almdal, K.; Mortensen, K.; Fredrickson, G. H. *J. Chem. Phys.* **1998**, *108*, 2989–3000.
(72) Vigild, M. E.; Chu, C.; Sugiyama, M.; Chaffin, K. A.; Bates, F. S. *Macromolecules* **2001**, *34*, 951–964.
(73) Mahanthappa, M. K.; Lim, L. S.; Hillmyer, M. A.; Bates, F. S. *Macromolecules* **2007**, *40*, 1585–1593.
(74) Helfand, E. *Macromolecules* **1975**, *8*, 552–556.
(75) Helfand, E.; Wasserman, Z. R. *Macromolecules* **1976**, *9*, 879–888.
(76) Hashimoto, T.; Shibayama, M.; Kawai, H. *Macromolecules* **1980**, *13*, 1237–1247.
(77) Semenov, A. N. *Sov. Phys. JTEP* **1985**, *61*, 733–742.
(78) Weidisch, R.; Michler, G. H.; Arnold, M. *Polymer* **2000**, *41*, 2231–2240.
(79) Koo, C. M.; Hillmyer, M. A.; Bates, F. S. *Macromolecules* **2006**, *39*, 667–677.
(80) Matsuo, M.; Ueno, T.; Horino, H.; Chujyo, S.; Asai, H. *Polymer* **1968**, *9*, 425–436.
(81) Beecher, J. F.; Marker, L.; Bradford, R. D.; Aggarwal, S. L. *Polym. Prepr.* **1969**, *8*, 1532.
(82) Phatak, A.; Lim, L. S.; Reaves, C. K.; Bates, F. S. *Macromolecules* **2006**, *39*, 6221–6228.
(83) Schmalz, H.; Böker, A.; Lange, R.; Kraush, G.; Abetz, V. *Macromolecules* **2001**, *34*, 8720–8729.

MA900183P